Loss mechanisms in high efficiency polymer solar cells

MacKenzie, R. C. I.; Balderrama, V. S.; Schmeisser, S.; Stoof, R.; Greedy, S.; Pallares, J.; Marsal, L. M.; Chanaewa, A.; von Hauff, E.L.

published in
Advanced Energy Materials
2016

DOI (link to publisher)
10.1002/aenm.201501742

document version
Early version, also known as pre-print

Polymer Solar Cells

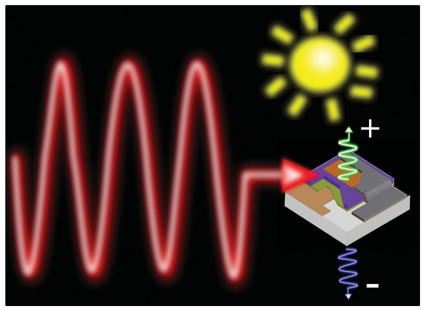

Air stable PTB7:$PC_{70}BM$ solar cells with efficiencies of 8% are demonstrated. The device employs a V_2O_5 anodic transport layer. Impedance spectroscopy is applied to confirm that the device contact interfaces in this architecture are stable under ambient conditions. Intensity modulated photocurrent spectroscopy is used to model the optoelectronic response of solar cell active layer as a function of aging.

ADVANCED ENERGY MATERIALS
www.advenergymat.de

Loss Mechanisms in High Efficiency Polymer Solar Cells

R. C. I. MacKenzie, V. S. Balderrama, S. Schmeisser, R. Stoof, S. Greedy, J. Pallarès, L. F. Marsal, A. Chanaewa, and E. von Hauff**

Performance losses and aging mechanisms are investigated in state-of-the-art PTB7:$PC_{70}BM$ solar cells. Inverted devices incorporating a vanadium pentoxide (V_2O_5) top contact have efficiencies of 8%. After aging the unencapsulated devices, no changes are observed in the open circuit voltage (V_{oc}) or short circuit current (J_{sc}); however, the fill factor (FF) drops from 0.7 to 0.61. An s-shape initially appears in the *J–V* curve after aging, which can be reduced by cycling through the *J–V* curve under illumination. This is discussed in context of the redox properties of V_2O_5. With impedance spectroscopy, it is demonstrated that changes to the contact interfaces are completely reversible and not responsible for the performance loss. Intensity modulated photocurrent spectroscopy combined with device modeling reveals that the loss in FF is due to trap formation in the active layer. Additionally it is observed that the performance of pristine devices is limited by optical absorption in the thin active layer and the build-up of space charge which hinders carrier extraction.

1. Introduction

Power conversion efficiencies of polymer solar cells have now surpassed 9%.[1–4] The rapid increase in performance has been largely due to the development of novel donor–acceptor polymers with broad optical absorption.[5] State of the art power conversion efficiencies have been achieved using blends of poly[[4,8-bis[(2-ethylhexyl)-oxy]benzo[1,2-b:4,5-b′]dithiophene-2,6-diyl][3-fluoro-2-[(2-ethylhexyl) carbonyl]-thieno[3,4-b]thiophenediyl]] (PTB7)[6] and phenyl-C71-butyric acid methyl ester ($PC_{70}BM$).[2,7]

Despite promising results, the performance of PTB7:$PC_{70}BM$ solar cells is limited by the thin active layer,[3] carrier selectivity at the contacts,[8] and rapid degradation of the active layer and contacts caused by exposure to ambient oxygen[9–11] and water vapor.[12] Although inverted solar cell architectures have demonstrated high efficiencies combined with relatively good stability, age-induced performance loss in high performance PTB7 solar cell architectures[2] has been reported, and the mechanisms are currently not well understood.

Identifying the origins of performance loss in solar cells is challenging because it involves differentiating between interfacial phenomena and bulk properties.[13] Frequency resolved optoelectronic techniques such as impedance spectroscopy[14] and intensity modulated photocurrent spectroscopy (IMPS)[15] are useful in discriminating between electronic processes in the active layer and at contact interfaces, and correlating these with device performance. In this work, we combine these techniques with device modeling to identify key loss processes and aging mechanisms in state-of-the-art PTB7-based inverted solar cells incorporating a V_2O_5 hole transport layer. After prolonged exposure to ambient conditions no change in the open circuit voltage (V_{oc}) or short circuit current density (J_{sc}) was observed. An s-shape is initially observed in the current density - voltage (*J–V*) characteristic, which can be reversed by cycling through the *J–V* curve under illumination. Subsequently, a small drop in the fill factor (FF) from the original value of 0.7 to 0.61 was observed. With impedance spectroscopy, we demonstrate that changes to the device interfaces are completely reversible, and that performance losses related to the FF are due to degradation of the organic active layer. The IMPS analysis reveals age-related trap formation in the active layer. Interestingly, the high density of traps does not appear to have a significant effect on performance. We attribute this phenomenon to slow carrier thermalization times.

2. Results

The device structure is depicted in **Figure 1**a. The PTB7:$PC_{70}BM$ active layer was sandwiched between an Indium tin oxide (ITO)/poly[(9,9-bis(3-(*N*,*N*-dimethylamino)propyl)-2,7-fluorene)-alt-2,7-(9,9–dioctylfluorene)] (PFN)[16] electron extracting contact

Dr. R. C. I. MacKenzie, Dr. S. Greedy
Faculty of Engineering
University of Nottingham
Nottingham NG7 2RD, UK
E-mail: roderick.mackenzie@nottingham.ac.uk
Dr. V. S. Balderrama, Prof. J. Pallarès, Prof. L. F. Marsal
Departament d'Enginyeria Electrònica Elèctrica i Automàtica
Universitat Rovira i Virgili
Avda. Països Catalans 26, 43007 Tarragona, Spain
S. Schmeisser
Institute of Physics
Albert-Ludwigs University of Freiburg
Hermann-Herder-Str. 3, 79104 Freiburg, Germany
R. Stoof, Dr. A. Chanaewa, Dr. E. von Hauff
Department of Physics and Astronomy
Physics of Energy
Amsterdam, Netherlands
E-mail: e.l.von.hauff@vu.nl

DOI: 10.1002/aenm.201501742

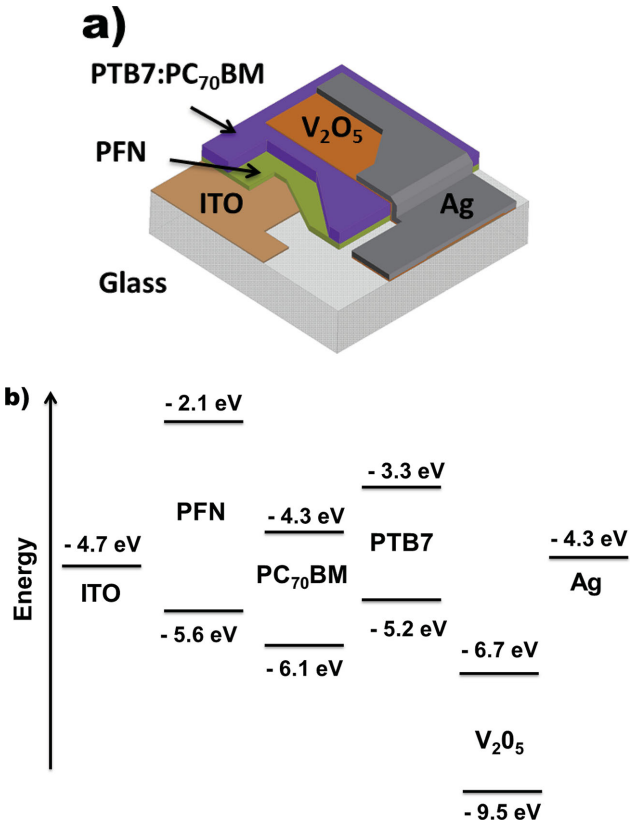

Figure 1. a) The solar cell architecture used in this study. b) Relative energy positions of the contact materials (ITO, PFN, V_2O_5, and Ag) and active layer (PTB7 and $PC_{70}BM$).

and a V_2O_5[17–21]/Ag hole extracting contact. The PFN and active layer were deposited using spin coating, while the V_2O_5 and silver (Ag) were deposited using thermal evaporation. The relative energy levels of the layers are shown in Figure 1b.[2,22] Impedance and IMPS measurements were carried out using a Metrohm Autolab. *J–V* measurements were carried out using a Keithley 2401 source measurement unit in combination with a solar simulator SS80 (Photo Emission Tech, Inc.). Full details of the fabrication and measurement process can be found in the Supporting Information.

A typical light *J–V* curve for a fresh PFN/PTB7:$PC_{70}BM$/V_2O_5/Ag device is shown in **Figure 2** (red dots). This cell has an efficiency of 8% (J_{sc} = 16.7 mA cm^{-2}, V_{oc} = 0.69 V, and FF = 0.7). The black symbols (Figure 2) represent the *J–V* curve of the same device after it has been exposed to air for four weeks (International Summit on OPV Stability ISOS standard D-1[23]). We observe an s-shape initially in the *J–V* characteristics after aging which can be eliminated by cycling through the *J–V* curve under illumination. After aging and *J–V* cycling, both J_{sc} and V_{oc} retain the initial values but the FF is reduced to 0.61.

Previously s-shaped *J–V* curves have been attributed to a reduction in charge extraction efficiency[24–28] due to the formation of an extraction barrier at the contacts.[29–31] Interesting, we also note that when the aged device is successively cycled through the *J–V* curve under illumination, the s-shape is reduced (Figure 2, gray symbols) and after 100 cycles the *J–V* curve fully recovers, except for the drop in FF. This suggests that *J–V* cycling

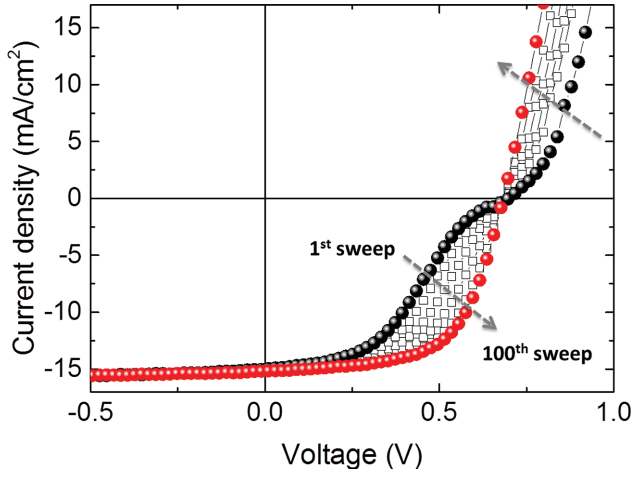

Figure 2. *J–V* characteristics of a solar cell exposed to ambient conditions for four weeks. The black symbols show the initial *J–V* curve, and gray symbols and arrows depict successive *J–V* cycles to recover the solar cell performance. The red symbols show the *J–V* characteristics after 100 sweeps.

under light exposure reduces the height of an extraction barrier within the device. Other reports have shown that PTB7:$PC_{70}BM$ blends are highly sensitive to photooxidation.[9,10] The fact that V_{oc} and J_{sc} do not change with aging, suggests that the V_2O_5 hole collection layer is at least partially encapsulating the active layer from irreversible degradation.[32] We attribute both the stability of the device architecture as well as the recovery of the *J–V* characteristics after aging to the redox properties of V_2O_5.

V_2O_5 is a well-known oxidizing agent, and oxygen vacancies in V_2O_5 are easily induced[12,33–36] via annealing[35,36] and environmental exposure.[12,22] The reduction of V^{5+} to lower oxidation states has been correlated with a decrease in the work function of V_2O_5 films,[22] which would represent an extraction barrier for holes from the solar cell. When the device is illuminated, however, electron injection from the conduction band of the V_2O_5 into the HOMO of the donor molecule subsequently reoxidizes the V_2O_5 thereby reducing the extraction barrier. Teran-Escobar et al. recently reported on a similar phenomenon and correlated the age and oxidation state of solution deposited V_2O_5 layers with the quality of the *J–V* characteristics of P3HT:PCBM solar cells.[12] The complete reversibility of the s-shape in the *J–V* of our solar cells compared to partial recovery observed in ref. [12] can be due to the difference in the properties and quality of thermally evaporated versus solution processed V_2O_5 layers. These results demonstrate the potential of achieving high stability in organic photovoltaics via chemical control[37] of the contact interfaces to tune extraction barriers.

To demonstrate the stability of the device interfaces and confirm that performance loss after aging is only related to changes in the active layer, we apply impedance spectroscopy. Impedance spectroscopy has previously been widely applied to study recombination, transport, and carrier extraction barriers in organic solar cells.[24,30,31,38–40] Measurements were performed under illumination on the pristine device (fresh), and on the degraded device after the s-shape had been eliminated from the *J–V* (aged).

Figure 3 shows the Cole–Cole representation of the impedance data taken under illumination from the fresh solar cell

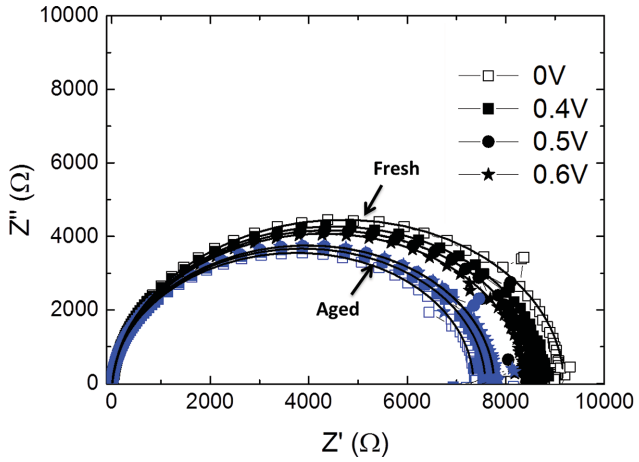

Figure 3. Cole–cole plots for the device under illumination before (black) and after (blue) aging are shown for applied DC voltages of 0, 0.4, 0.5, and 0.6 V.

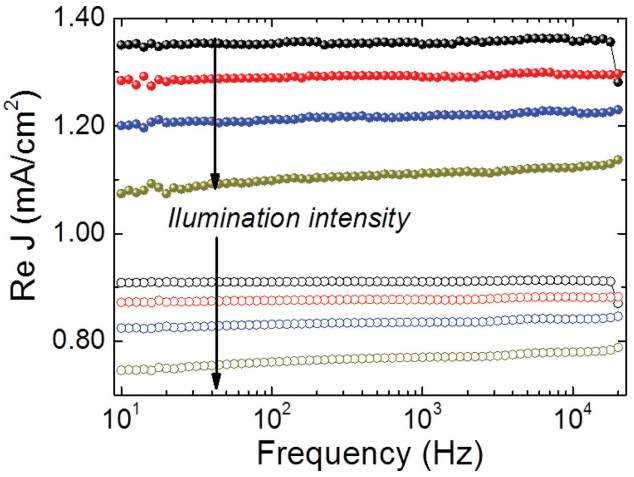

Figure 4. Re(J) versus frequency before (closed symbols) and after (open symbols) aging for illumination intensities of 50, 100, 150, and 200 mW cm^{-2} with a red LED (627 nm). The arrows indicate increasing background light intensity.

(black) and after (blue) aging. It can be seen that both the real (Z') and imaginary (Z'') impedance values are slightly lower for the aged device. Furthermore, it can be seen that the impedance increases minimally with applied DC voltage after aging. Interestingly, we do not observe features in the impedance spectra which are characteristic of contact corrosion impeding charge extraction, i.e., peaks in the dielectric loss spectra and/or the emergence of new, high frequency features,[24,31,41] indicating that after voltage cycling the device, the extraction barrier resulting in the s-shape is eliminated.

To better understand the impedance spectra, we fit the data with an equivalent circuit model consisting of three resistor-capacitor (RC) elements.[38] The solid lines in Figure 3 show the fits. The details of this procedure can be found in the Supporting Information. This allowed us to correlate changes in the impedance spectra before and after aging with the optoelectronic response of physical sites in the solar cell, i.e., the contact interfaces and the bulk active layer.[38,42] From this analysis, we observe a decrease in the series resistance of the device after aging which we attribute to changes in the electronic propertise of the V_2O_5 layer. Additionally there is a decrease in the resistance of the RC element associated with the response of the active layer. We do not observe any age-induced changes in the circuit elements associated with the contact interfaces. This suggests that changes in device response after aging are only related to the active layer and that changes to the contact interfaces in this device architecture are completely reversible.

To gain insights into degradation of the active layer resulting in the decrease in the FF we employ IMPS. IMPS has been widely applied to study electrochemical systems[15] such as dye sensitized solar cells,[43] but rarely to study organic photovoltaics.[44–47] In this measurement a small optical AC perturbation is superimposed on the background light intensity, causing periodic variations in carrier density. By monitoring the changes in the photocurrent collected at the contacts as a function of light modulation, transient phenomena such as trapping, recombination, and charge transfer at material interfaces can be probed as a function of carrier density. The resulting change in the photocurrent density (J) is fit with equation

$$J(t) = J\exp(i\omega t - \Phi) \tag{1}$$

where J represents the magnitude of the change in photocurrent and Φ represents the phase shift between the light modulation and the current response.

In the following measurements, the cell was kept at short circuit and illuminated with a red light emitting diode (LED) (627 nm) with background bias light intensities of 50, 100, 150, and 200 mW cm^{-2}.

Figure 4 depicts the real (Re) component of J versus frequency as a function of background light intensity, measured before (closed symbols) and after aging (open symbols). Re(J) decreases with increasing illumination intensity. At higher light intensities carrier density is higher and recombination increases, and the sinusoidal perturbation produces less change in the current density collected at the contacts. In addition, a weak positive dependence of Re(J) on frequency is observed. A comparison of the spectra reveals that the optical perturbation produces less change in J after aging.

The imaginary component of J, Im(J), is plotted in **Figure 5** (a) before and (b) after aging. Im(J) reflects how the generated photocurrent leads or lags the modulation in light intensity. The trend of the Im(J) spectra of the solar cell before and after aging are very comparable, except in the high frequency regime. Im(J) values are more than ten times lower than Re(J) values, indicating that the phase shift between photogeneration and charge extraction in the device is small. Interestingly, Im(J) is mostly positive, particularly at low frequencies and with increasing light intensity. This indicates that the maximum in extracted photocurrent precedes that of the photoflux, i.e., the device produces a maximum current before the modulated light intensity peaks. Im(J) decreases gradually between 10 Hz and 1 kHz, before peaking around 3 kHz. Before aging, at frequencies above 4 kHz, the Im(J) spectra decreases and becomes negative. After aging the device, however, Im(J) increases at higher frequencies.

Previously, positive values of Im(J) have been attributed to degradation-induced trap formation.[46] However, we would

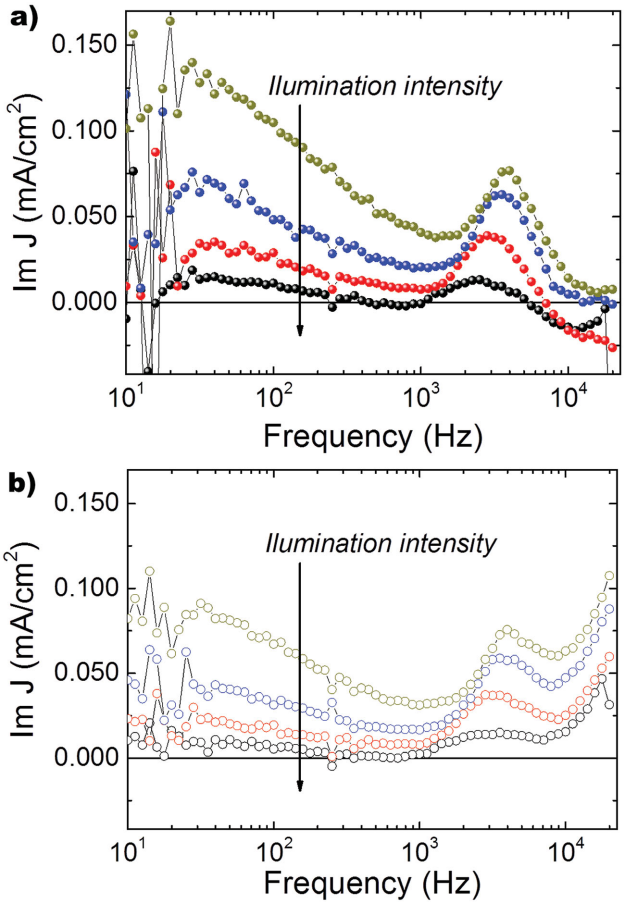

Figure 5. Im(*J*) spectra a) before and b) after aging at illumination intensities of 50, 100, 150, and 200 mW cm^{-2} with a red LED (623 nm).

not expect to see this in fresh, high efficiency devices. Furthermore, the gradual drop in Im(*J*) and the peak at 3 kHz have not been previously reported. Difficulties in interpreting IMPS data from organic photovoltaics due to the complex interfacial phenomena combined with wide range of time scales for key electronic processes have limited its application in the field to date.[45] Therefore, to analyze our results, we developed a Shockley–Read–Hall based[48,49] drift-diffusion model to quantify the features in the spectra.

The model uses an effective medium approximation to describe the electrical characteristics of the device.[50] The model solves Poisson's equation, the electron/hole drift diffusion equations and the carrier continuity equations in 1D from the cathode to the anode. The energetic distribution of trap states in energy space is assumed to be exponential and the optical profile within the device is calculated using the transfer matrix method (see the Supporting Information for details).

The device model was fit self-consistently to both the illuminated *J–V* curve and two cycles of the IMPS response of the device, at 39 Hz and at 2818.4 Hz. In order to keep the interpretation of the results as simple as possible and reduce the number of fitting parameters, the model parameters were kept symmetric. Once the model was calibrated to the experimental data, we asked the model to predict the shape of the Re(*J*) and Im(*J*) spectra from 10 Hz to 5 kHz (**Figure 6**). A comparison between the experimental (Figure 4) and simulated (Figure 6a) Re(*J*) spectra reveals the same trend; a gradual increase in Re(*J*) with frequency and a decrease in signal with increasing light intensity.

In the case of Im(*J*), experimental (Figure 5) and simulated (Figure 6b) spectra both show a positive photocurrent. This indicates that when responding to a sinusoidal optical excitation, the device reaches its maximum efficiency and produces most current before the light intensity is at its maximum. This is a counterintuitive effect and is not expected in high efficiency devices at low frequencies. For frequencies which approach the DC case, it would be expected that changes in the light intensity result in immediate changes in the photocurrent. Time delays between optical modulation and photocurrent response at low frequencies indicates loss processes even in the fresh devices. The increase in the magnitude of Im(*J*) with increasing light intensity suggests processes dependent on illumination and/or charge density.

Increasing the carrier density in low mobility organic materials is expected to lead to the build-up of space-charge. With our model we were able to produce a positive Im(*J*) current at low frequencies by using parameters which encouraged the formation of nonuniform and transient spatial distributions of charge within the device, resulting in band bending which hinders charge extraction.[15] This resulted in a peak in photocurrent generation and device efficiency before the modulated light reached its maximum intensity. The effect could be turned on by increasing the energetic distribution of trap states while

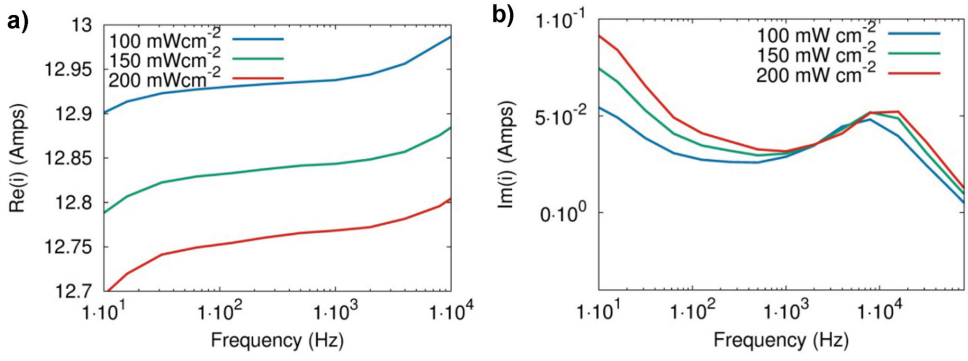

Figure 6. Simulated a) Re(*J*) and b) Im(*J*) response of the device plotted as a function of light intensity.

keeping the recombination rate low. The effect could be turned off by artificially increasing the permittivity of the material in the simulation to prevent band bending (see the Supporting Information).

We now consider the optical properties of the organic active layer as a function of light intensity. Im(J) decreases between 10 Hz and 1 kHz (Figure 5). Interestingly, we were unable to reproduce this by varying the electrical parameters in the model alone. Furthermore, we were unable to self-consistently fit the J–V curve while simultaneously producing the experimentally observed peak above 1 kHz in the Im(J) spectra. In order to self-consistently reproduce all the experimental trends in the Im(J) spectra with the model, we had to allow the optical absorption of the active layer to decrease as light intensity was increased, simulating reversible optical bleaching. Under increasing illumination intensity, bleaching of the active layer occurs as higher energy states are filled with charge, depleting the ground state and making the promotion of further carriers to higher states unlikely. Once easily excitable charge occupies these higher states, α decreases.

We modeled this effect by reducing the optical absorption coefficient α of the active layer as a function of local free carrier density

$$\alpha(x) = \alpha_0(x) + \rho\left(n_f^0(x)\, p_f^0(x) - n_f(x)\, p_f(x)\right) \quad (2)$$

where $n_f^o(x)$ and $p_f^o(x)$ are spatially dependent density of free carriers at equilibrium in the dark, $n_f(x)$ and $p_f(x)$ are the density of free carriers out of equilibrium.

We then examined the distinctive peak in the Im(J) spectra (Figure 5) at 3 kHz. The position of this peak can be shifted by altering the carrier capture and recombination cross sections. This peak is still observed even if the permittivity of the medium is increased to a very high value to turn off electrostatic effects and band bending. We explain this effect by considering that increasing the frequency of light modulation leads to increasing lag in the carrier recombination with respect to carrier generation, as the occupation of trap states is retarded at higher frequencies. As the frequency of light modulation approaches 3 kHz the trapped carrier population is 180° out of phase with carrier generation, resulting from carrier recombination being faster than carrier thermalization (see the Supporting Information).

We finally turn our attention to the differences in the high frequency behavior of the Im(J) spectra before and after aging. Before the device is aged (Figure 5a,b), Im(J) values continually decrease at frequencies above 3 kHz and become negative. Negative Im(J) values occur when photogenerated charge cannot be transported to the contacts as fast as the optical field is changing. Furthermore, because the optical field is changing so fast, there is not enough time during the IMPS oscillation to allow a build-up of space charge to hinder extraction. Thus a negative imaginary IMPS signal indicates that the transit time of the carriers is longer than the period of the modulating light. After aging the device (Figure 4b) Im(J) continually increases at higher frequencies. This behavior could be reproduced in the model by increasing the density of trap states from 5×10^{25} to 5×10^{26} m^{-3} eV^{-1} (**Figure 7**) but not by changing recombination rates or carrier mobility values.

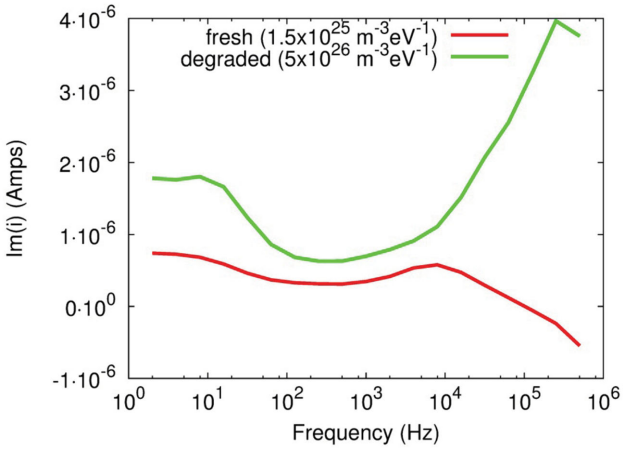

Figure 7. The simulated IMPS spectra of the fresh device (red line) and of a device with an increased number of trap states (green line).

Lastly it should be noted that none of the features in the Im(J) spectra could be reproduced by introducing extraction barriers at the device interfaces. This is in agreement with the results from the impedance analysis. Based on the impedance and IMPS results, the slight loss in FF after ambient exposure is attributed to low density trap formation in the organic active layer.

We are able to apply IMPS together with device modeling to quantify loss processes in high efficiency, pristine PTB7:PC_{70}BM solar cells. On the one hand, low carrier mobility, likely in the polymer phase, results in the build-up of space charge in the active layer, preventing the extraction of charge from the device. The poor transport properties of PTB7 layers is a reason why optimized solar cells based on PTB7 employ extremely thin active layers.[2,8] We confirm, however, that the photocurrent in the device is ultimately determined by limitations in the optical absorption of these thin active layers.[3] We note that the effects are minimal under lower illumination (very low Im(J) values) but become increasingly apparent as the intensity is increased.

After aging the device, the trap density within the active layer is found to increase by over an order of magnitude. Interestingly this does not affect carrier mobility values or recombination rates, and as a result, the photocurrent does not decrease. This could be due to the charge carrier capture cross section being over three orders of magnitude smaller than for a material system with molecularly ordered domains such as P3HT:PCBM.[51] The high efficiencies achieved with PTB7:PC_{70}BM blends have been attributed to minimizing the domain sizes of the polymer and fullerene phases to facilitate efficient charge transfer.[52] Further, the PTB7:PC_{70}BM active layer is kept thin (<100 nm) to minimize nongeminate recombination losses in the amorphous polymer phase.[53,54] In contrast, solar cells based on P3HT:PCBM do not demonstrate pronounced dependence on the thickness of the active layer.[8]

In contrast to the well-studied P3HT:PCBM system,[55] underlying molecular mechanisms related to degradation of the PTB7:PC_{70}BM blend are not yet well understood.[56] Recently Razzell-Hollis et al.[9] applied Raman spectroscopy

to monitor molecular level changes in PTB7:PC70BM blends after photodegradation. They found that photooxidation is a two-step process and applied density functional theory (DFT) to find that hydroxyl formation on the benzodithiophene (BDT) unit was linked as a probable cause connected to final, irreversible degradation. Cox et al.[10] used frequency modulated electrostatic force microscopy on PTB7:$PC_{70}BM$ blends and showed that photodegradation results in local variations in the measured surface potential of the blend on the scale of 40 nm. The commonly used additive 1,8-diiodooctane (DIO) used in high efficiency blends stabilized the blends against degradation and prevented larger scale damage. Based on these results, we attribute the observed performance loss in our PTB7:$PC_{70}BM$ solar cells to molecular scale changes to the polymer backbone, and not due to larger scale morphological changes of the blend.

3. Conclusions

We investigate loss mechanisms in efficient inverted PTB7:$PC_{70}BM$ solar cells. Upon exposure to ambient conditions for several weeks, an s-shape emerges in the *J–V* curve. Cycling through the *J–V* curve under illumination leads to reduction of the s-shape and recovery of the *J–V* curve. No losses in V_{oc} or J_{sc} due to aging were observed; however, the FF drops from 0.7 to 0.61. Both impedance spectroscopy and IMPS demonstrated that after *J–V* cycling there was no significant extraction barrier present in the device, indicating that changes to the contact interfaces are completely reversible. By applying a Shockley–Read–Hall drift-diffusion model together with IMPS measurements, we investigate processes related to performance loss in the active layer. We demonstrate that the intensity-dependent positive Im(*J*) response of the IMPS spectra at low frequencies indicates reversible optical bleaching of the thin active layer as well as band bending effects. Traps are formed in the active layer upon aging; however, they do not significantly decrease device performance. We attribute this to a slow carrier thermalization rate in the PTB7 material system. These results reveal that key performance limiting mechanisms in state of the art organic solar cells.

Supporting Information

Supporting Information is available online from the Wiley Online Library or from the author.

Acknowledgements

S.S., A.C., and E.V.H. acknowledge support from Fraunhofer Institute of Solar Energy Systems and the German Science Foundation (DFG). A.C. and E.v.H. additionally thank the Foundation for Fundamental Research on Matter (FOM) (V0714M-13MV60) from the Netherlands Organization for Scientific Research (NWO) for support. V.S.B., J.P., and L.F.M. thank the Spanish Ministry of Economy and Competitiveness TEC2012-34397, Catalan Government AGAUR 2014SGR1433, and the ICREA Academia Award.

Received: August 31, 2015
Revised: November 4, 2015
Published online:

[1] M. A. Green, K. Emery, Y. Hishikawa, W. Warta, E. D. Dunlop, *Prog. Photovolt: Res. Appl.* **2014**, *22*, 701.
[2] Z. He, C. Zhong, S. Su, M. Xu, H. Wu, Y. Cao, *Nat. Photonics* **2012**, *6*, 593.
[3] Y. Liu, J. Zhao, Z. Li, C. Mu, W. Ma, H. Hu, K. Jiang, H. Lin, H. Ade, H. Yan, *Nat. Commun.* **2014**, *5*, 5293.
[4] I. Etxebarria, J. Ajuria, R. Pacios, *Org. Electron.* **2015**, *19*, 34.
[5] G. Li, R. Zhu, Y. Yang, *Nat. Photonics* **2012**, *6*, 153.
[6] Y. Liang, Z. Xu, J. Xia, S.-T. Tsai, Y. Wu, G. Li, C. Ray, L. Yu, *Adv. Mater.* **2010**, *22*, E135.
[7] L. Lu, L. Yu, *Adv. Mater.* **2014**, *26*, 4413.
[8] A. Guerrero, N. F. Montcada, J. Ajuria, I. Etxebarria, R. Pacios, G. Garcia-Belmonte, E. Palomares, *J. Mater. Chem. A* **2013**, *1*, 12345.
[9] J. Razzell-Hollis, J. Wade, W. C. Tsoi, Y. Soon, J. Durrant, J.-S. Kim, *J. Mater. Chem. A* **2014**, *2*, 20189.
[10] P. A. Cox, D. A. Waldow, T. J. Dupper, S. Jesse, D. S. Ginger, *ACS Nano* **2013**, *7*, 10405.
[11] E. A. A. Arbab, B. Taleatu, G. T. Mola, *J. Mod. Opt.* **2014**, *61*, 1749.
[12] P. Romero-Gomez, R. Betancur, A. Martinez-Otero, X. Elias, M. Mariano, B. Romero, B. Arredondo, R. Vergaz, J. Martorell, *Sol. Energy. Mater. Sol. Cells* **2015**, *37*, 44.
[13] M. Jorgensen, K. Norrman, S. Gevorgyan, T. Tromholt, B. Andreasen, F. C. Krebs, *Adv. Mater.* **2012**, *24*, 580.
[14] J. R. Macdonald, *Ann. Biomed. Eng.* **1992**, *20*, 289.
[15] E. A. Ponomarev, L. M. Peter, *J. Electroanal. Chem.* **1995**, *396*, 219.
[16] F. Huang, H. B. Wu, D. L. Wang, W. Yang, Y. Cao, *Chem. Mater.* **2004**, *16*, 708.
[17] G. Teran-Escobar, J. Pampel, J. M. Caicedo, M. Lira-Cantu, *Energy Environ. Sci.* **2013**, *6*, 3088.
[18] M. Terai, K. Fujita, T. Tsutsu, *Jpn. J. Appl. Phys.* **2005**, *44*, L1059.
[19] K. Zilberberg, S. Trost, H. Schmidt, T. Riedl, *Adv. Energy Mater.* **2011**, *1*, 377.
[20] M. G. Helander, Z. B. Wang, M. T. Greiner, J. Qiu, Z. H. Lu, *Appl. Phys. Lett.* **2009**, *95*, 083301.
[21] V. Shrotriya, G. Li, Y. Yao, C.-W. Chu, Y. Yang, *Appl. Phys. Lett.* **2006**, *88*, 073508.
[22] J. Meyer, K. Zilberberg, T. Riedl, A. Kahn, *J. Appl. Phys.* **2011**, *110*, 033710.
[23] M. Reese, S. A. Gevorgyan, M. Jorgensen, E. Bundgaard, S. R. Kurtz, D. S. Ginley, D. C. Olson, M. T. Lloyd, P. Morvillo, E. A. Katz, A. Elschner, O. Haillant, T. R. Currier, V. Shrotriya, M. Hermenau, M. Riede, K. R. Kirov, G. Trimmel, T. Rath, O. Inganas, F. Zhang, M. Andersson, K. Tvingstedt, M. Lira-Cantu, D. Laird, C. McGuiness, S. Gowrisanker, M. Pannone, M. Xiao, J. Hauch, R. Steim, D. M. DeLongchamp, R. Rosch, H. Hoppe, N. Espinosa, A. Urbina, G. Yaman-Uzunoglu, J. B. Bonekamp, A. J. J. M. van Breemen, C. Girotto, E. Voroshazi, F. C. Krebs*Sol. Energy Mat. Sol. Cells* **2011**, *95*, 1253.
[24] M. Glatthaar, M. Riede, N. Keegan, K. Sylvester-Hvid, B. Zimmermann, M. Niggemann, A. Hinsch, A. Gombert, *Sol. Energy Mater. Sol. Cells* **2007**, *91*, 390.
[25] A. Wagenpfahl, D. Rauh, M. Binder, C. Deibel, V. Dyakonov, *Phys. Rev. B* **2010**, *82*, 115306.
[26] W. Tress, K. Leo, M. Riede, *Adv. Funct. Mater.* **2011**, *21*, 2140.
[27] B. Y. Finck, B. J. Schwartz, *Appl. Phys. Lett.* **2013**, *103*, 053306.
[28] L. Sims, U. Hörmann, R. Hanfland, R. C. I. MacKenzie, F. R. Kogler, R. Steim, W. Brütting, P. Schilinsky, *Org. Electron.* **2014**, *15*, 2862.
[29] E. Voroshazi, B. Verreeta, A. Buric, R. Müller, D. Di Nuzzo, P. Heremans, *Org. Electron.* **2011**, *12*, 736.
[30] B. Ecker, J. Nolasco, J. Pallarés, L. Marsal, J. Posdorfer, J. Parisi, E. von Hauff, *Adv. Funct. Mater.* **2011**, *21*, 2705.
[31] B. Ecker, J. Posdorfer, E. von Hauff, *Sol. Energy Mater. Sol. Cells* **2013**, *116*, 176.

[32] T. Yanagidate, S. Fujii, M. Ohzeki, Y. Yanagi, Y. Arai, T. Okukawa, A. Yoshida, H. Kataura, Y. Nishioka, *Jpn. J. Appl. Phys.* **2014**, *53*, 02BE05.
[33] R. Rambez, B. Casal, L. Utrera, E. Ruiz-Hitzky, *J. Phys. Chem.* **1990**, *94*, 8960.
[34] Q.-H. Wua, A. Thissen, W. Jaegermann, M. Liu, *Appl. Surf. Sci.* **2004**, *236*, 473.
[35] D. S. Su, R. Schlögl, *Catal. Lett.* **2002**, *83*, 115.
[36] S. Guimond, J. M. Sturm, D. Göbke, Z. Romanyshyn, M. Naschitzki, H. Kuhlenbeck, H.-J. Freund, *J. Phys. Chem. C* **2008**, *112*, 11835.
[37] S. R. Cowan, P. Schulz, A. J. Giordano, A. Garcia, B. A. MacLeod, S. R. Marder, A. Kahn, D. S. Ginley, E. L. Ratcliff, D. C. Olson, *Adv. Funct. Mater.* **2014**, *24*, 4671.
[38] A. Guerrero, N. F. Montcada, J. Ajuria, I. Etxebarria, R. Pacios, G. Garcia-Belmonte, E. Palomares, *J. Mater. Chem. A* **2013**, *1*, 12345.
[39] B. Ecker, R. Steim, H. J. Egelhaaf, J. Parisi, E. von Hauff, *J. Phys. Chem.* **2012**, *116*, 16333.
[40] J. Bisquert, L. Bertoluzzi, I. Mora-Sero, G. Garcia-Belmonte, *J. Phys. Chem. C* **2014**, *118*, 18983.
[41] B. Ecker, R. Steim, H. J. Egelhaaf, J. Parisi, E. von Hauff, *J. Phys. Chem.* **2012**, *116*, 16333.
[42] D. A. Harrington, P. van den Driessche, *Electrochim. Acta* **2011**, *56*, 8005.
[43] P. E. de Jongh, D. Vanmaekelbergh, *Phys. Rev. Lett* **1996**, *77*, 3427.
[44] T. Oekermann, D. Schlettwein, N. I. Jaeger, *J. Phys. Chem. B* **2001**, *105*, 9524.
[45] P. M. DiCarmine, O. A. Semenikhin, *Electrochim. Acta* **2008**, *53*, 3744.
[46] Y. T. Set, M. D. Heinemann, E. Birgersson, J. Luther, *J. Phys. Chem. C* **2013**, *117*, 7993.
[47] S. Cho, K.-D. Kim, J. Heo, J. Y. Lee, G. Cha, B. Y. Seo, Y. D. Kim, Y. S. Kim, S. Y. Choi, D. C. Lim, *Sci. Rep.* **2014**, *4*, 4306.
[48] W. Shockley, W. T. Read, *Phys. Rev.* **1952**, *87*, 835.
[49] R. C. I. MacKenzie, C. G. Shuttle, M. L. Chabinyc, J. Nelson, *Adv. Energy Mater.* **2012**, *2*, 662.
[50] L. J. A. Koster, E. C. P. Smits, V. D. Mihailetchi, P. W. M. Blom, *Phys. Rev. B* **2005**, *72*, 085205.
[51] R. C. I. MacKenzie, C. G. Shuttle, M. L. Chabinyc, J. Nelson, *Adv. Energy Mater.* **2012**, *6*, 662.
[52] B. A. Collins, Z. Li, J. R. Tumbleston, E. Gann, C. R. McNeill, H. Ade, *Adv. Energy Mater.* **2013**, *3*, 65.
[53] M. R. Hammond, R. J. Kline, A. A. Herzing, L. J. Richter, D. S. Germack, H.-W. Ro, C. L. Soles, D. A. Fischer, T. Xu, L. Yu, M. F. Toney, D. M. DeLongchamp, *ACS Nano* **2011**, *5*, 8248.
[54] Y. Liu, J. Zhao, Z. Li, C. Mu, W. Ma, H. Hu, K. Jiang, H. Lin, H. Ade, H. Yan, *Nat. Commun.* **2014**, *5*, 5293.
[55] F. Deschler, A. De Sio, E. von Hauff, P. Kutka, T. Sauermann, H.-J. Egelhaaf, J. Hauch, E. Da Como, *Adv. Funct. Mater.* **2012**, *22*, 1461.
[56] S. Shah, R. Biswas, *J. Phys. Chem. C* **2015**, *119*, 20265.